

Hyperparameter-free and Explainable Whole Graph Embedding

Hao Wang, Yue Deng, Linyuan Lü, and Guanrong Chen

Abstract—Many real-world complex systems can be described as graphs. For a large-scale graph with low sparsity, a node’s adjacency vector is a long and sparse representation, limiting the practical utilization of existing machine learning methods on nodal features. In practice, graph embedding (graph representation learning) attempts to learn a lower-dimensional representation vector for each node or the whole graph while maintaining the most basic information of graph. Since various machine learning methods can efficiently process lower-dimensional vectors, graph embedding has recently attracted a lot of attention. However, most node embedding or whole graph embedding methods suffer from the problem of having more sophisticated methodology, hyperparameter optimization, and low explainability. This paper proposes a hyperparameter-free, extensible, and explainable whole graph embedding method, combining the DHC (Degree, H-index and Coreness) theorem and Shannon Entropy (E), abbreviated as DHC-E. The new whole graph embedding scheme can obtain a trade-off between the simplicity and the quality under some supervised classification learning tasks, using molecular, social, and brain networks. In addition, the proposed approach has a good performance in lower-dimensional graph visualization. The new methodology is overall simple, hyperparameter-free, extensible, and explainable for whole graph embedding with promising potential for exploring graph classification, prediction, and lower-dimensional graph visualization.

Index Terms—Graph Embedding; H-index; Entropy; Extensible; Classification.

I. INTRODUCTION

GRAPH (networks) can be used to describe the connections or associations between objects, which are ubiquitous in our daily lives. Examples include social networks,

Hao Wang and Yue Deng contributed equally to this work.

This work is supported by the National Natural Science Foundation of China (Nos. 61673150, 11622538), the Science Strength Promotion Program of the University of Electronic Science and Technology of China (No. Y030190261010020), and the China Scholarship Council (No. 201906070121). (Corresponding author: Linyuan Lü.)

Hao Wang and Yue Deng is with the Institute of Fundamental and Frontier Sciences, University of Electronic Science and Technology of China, Chengdu 611731, P. R. China, and also with Yangtze Delta Region Institute (Huzhou), University of Electronic Science and Technology of China, Huzhou 313001, P. R. China (e-mail: h.wang.psy@gmail.com; 201921210214@std.uestc.edu.cn).

Linyuan Lü is with the Institute of Fundamental and Frontier Sciences, University of Electronic Science and Technology of China, Chengdu 611731, P. R. China, and also with Yangtze Delta Region Institute (Huzhou), University of Electronic Science and Technology of China, Huzhou 313001, P. R. China, and also with Beijing Computational Science Research Center, Beijing 100193, P. R. China (e-mail: linyuan.lv@uestc.edu.cn).

Guanrong Chen is with the Department of Electrical Engineering, City University of Hong Kong, Hong Kong 999077, P. R. China (e-mail: eegchen@cityu.edu.hk).

Data and codes are freely available at <https://github.com/HW-HaoWang/DHC-E>.

citation networks, knowledge graphs, brain networks, etc. Graph analysis helps explore hidden information in complex systems and perform link prediction, node classification [1], clustering [2], visualization [3], and for understanding brain disorders [4]. In graph analysis, it is observed that, some large graphs are with small sparsity, where each node has only a few edges, resulting in a long nodal feature vector with many zeros [5], thereby causing traditional graph analytic methods high computation cost. To address this issue, some graph embedding methods have been proposed [6], [7], [8], which learn and reduce the node or whole graph features to a lower-dimensional vector and maximally preserve the original graph properties.

Before 2000, the main effort on network feature learning was dimension reduction of higher-dimensional data. Traditional methods include principal component analysis (PCA) [9], linear discriminant analysis (LDS) [10], multiple dimensional scaling (MDS) [11], etc. However, they are linear methods, which do not always perform well when there are nonlinear relationships within datasets. Subsequently, some other dimension reduction methods came about around 2000, among which popular ones were isometric mapping (IsoMap) [12] and Laplacian eigenmaps (LLE) [13]. Both IsoMap and LLE were manifold learning. From a more practical perspective, in 2013 word2vec [14] was developed using the SkipGram [15] model to learn lower-dimensional vector representations of words (word embedding). The excellent performance of word2vec promoted a wave of activities on embedding learning from the scientific communities. Based on the output features, one may classify the current graph embedding methods into four categories: node embedding [16], edge embedding [17], substructure embedding [18], and whole graph embedding [19].

Node embedding learns node feature while preserving the graph structure, in the sense that nodes close to each other in the graph will be close to each other in the embedding space. Edge embedding represents edge information as a lower-dimensional vector, which benefits edge (node pairs) related graph analysis, such as knowledge graph entity or relation prediction, link prediction, etc. Substructure embedding considers higher-order relations or subgraphs within the graph, learns to reduce the local community structure into a lower-dimensional representation vector, and helps better understand the relationships among different communities. Whole graph embedding, which learns a single vector of fixed length for the whole graph, provides a straightforward and efficient approach to calculating the graph similarity and classification. As mentioned above, node embedding methods are popular

in the literature. However, some practical applications require information at a higher level of granularity, for which one would turn to whole graph embedding.

Several whole graph embedding methods have been proposed. A typical one is the family of graph spectral distances (FGSD), which calculates the Moore-Penrose spectrum of the normalized Laplacian and uses the histogram of the spectral features as a whole graph representation [20]. Graph2vec [19] algorithm uses unsupervised methods to derive fixed-length task-agnostic embeddings of graphs and shows good performance in graph classification. Network Laplacian Spectral Descriptor (NetLSD) calculates the heat kernel trace of the normalized Laplacian matrix over a vector of time scales, which is a permutation- and size-invariant, scale-adaptive graph embedding [21]. Invariant graph embedding (IGE) computes a mixture of spectral and node embedding based features and pools node feature embedding to create graph descriptors [22]. Graph and Line graph to vector (GL2vec) complements either the edge label information or the structural information which Graph2vec missed [23].

However, to date, the aforementioned advanced approaches are mathematically intractable, sophisticated, and challenging to interpret, and suffer hyperparameter selection problems in comparing different graphs. Moreover, these algorithms are lacking evaluation on biological systems like brain networks. Thus, it is desirable to provide hyperparameter-free, easy-to-understand, explanatory, and extensible methods to make the graph embedding applicable for more disciplines. Based on the DHC and entropy, in this paper, we propose a simple, hyperparameter-free whole graph embedding method, and we examine its accuracy and effectiveness by comparing it with four state-of-the-art whole graph embedding methods, using modeled network, small molecules network, social network, brain network, and computer vision network. Our DHC-E method shows a better trade-off between complexity and good performance than baseline methods on various benchmark datasets.

Our main contributions are summarized as follows:

- 1) We develop a simple, hyperparameter-free, and extensible graph embedding method and provide python and MATLAB codes with detailed instructions.
- 2) We compare our method with four state-of-the-art graph embedding methods for network classification and offer practical suggestions for choosing appropriate embedding method for specific applications.
- 3) We successfully apply the new graph embedding method to brain networks in distinguishing autism participants with typical controls, extending the experiment to intelligent systems and make the brain morphological network available as a candidate benchmark dataset for evaluating the performance of future algorithms.
- 4) Our DHC-E graph embedding can achieve a good trade-off between the model complexity and effectiveness, and can combine with other graph embeddings to improve the performance of graphs classification. The algorithm is simple and effective, without the need to set any hyperparameter. It can be widely used for other disciplines.

The remaining of the article is organized as follows: In section II, we present some preliminaries, including a short introduction to graph, DHC metric, Shannon Entropy, and whole graph embedding. In section III, we present the derivation of DHC-E and apply different datasets to test the effectiveness of our method on graph classification tasks. We utilize four state-of-the-art effective complex models that at least need two hyperparameters as our baseline. In section IV, we use both simulated and empirical data to test the graph classification performance of our model against four baseline models. We also evaluate the stability and time complexity of all models. Furthermore, we combine our model with each baseline to test whether integration features can improve the graph classification performance. In addition, we use the DHC-E features to demonstrate an exploratory application in lower-dimension graph visualization. In section V, we provide a summary and present a vision for developing simple and effective graph embedding methods.

II. PRELIMINARIES

In this section, some preliminaries are presented, preparing for the technical development of the paper.

A. Graph

Complex systems in the real world usually comprise a set of interacted *objects* (or *components*), which can be represented by a graph [24] with objects being *nodes* (also called *vertices*) and their interactions (or relations) being *edges*. Mathematically, a graph is denoted by $G = (V, E)$, where V is the set of nodes and $E \subseteq (N \times N)$ is the set of edges. The edges of G can be weighted or unweighted, and directed or undirected. This paper only considers unweighted and undirected graphs with no self-loops or multiple edges.

B. Degree, H-index and coreness

The distribution of *vital nodes* determines the structural features of a graph and reveals the underlying dynamic mechanism of complex systems [25]. In the past two decades, identifying vital nodes in graphs has been attracting increasing attention from research communities, and it also has been proved to have many promising applications in practice, such as identifying innovation performance [26] and crucial brain regions [27], [28]. Many metrics for vital node identification [29] have been proposed, among which, the degree, H-index, and coreness are three widely used ones.

The *degree*, in particular, measures a node's influence in a straightforward way. A node with a higher degree indicates that it is connected with more nodes in the graph. The *H-index* (short for *Hirsch index*) [30] of a node in the graph is defined as the maximum value h such that there exist at least h neighbors who have a degree no less than h [31]. The *coreness* further takes the location of a node in the graph into account to measure its influence based on the k -core decomposition process [32]. A larger coreness of a node indicates that it is located more centrally in the graph. A schematic is shown illustration in Fig. 1 to explain how to calculate the three metrics for a given graph.

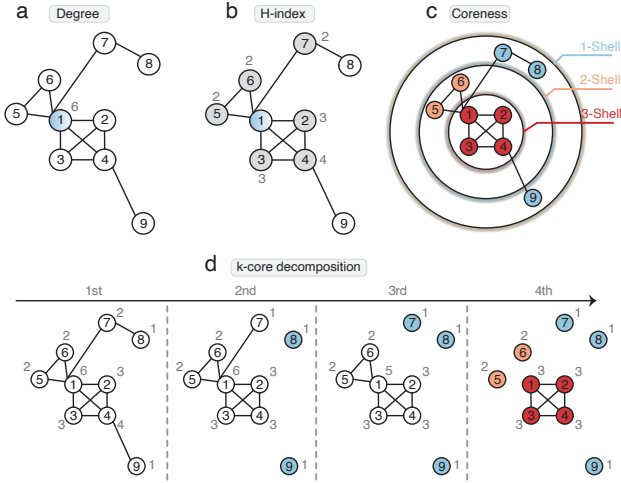


Fig. 1. **Illustration of calculating the nodal degree, H-index and coreness in a graph.** **a**, The degree of node 1 is six because it is connected with six nodes in the graph. **b**, After obtaining the degrees of the neighbors of node 1, it can be calculated that the H-index of node 1 is three. The same goes for other nodes in the graph. **c**, The coreness of nodes can be calculated by implementing the k -core decomposition on the graph. During the k -core decomposition process, each node is assigned a shell layer, called the node's coreness. The k -core decomposition process is illustrated in **d**. Specifically, the nodes with a degree of 1 (i.e., nodes 8 and 9) are initially removed. Since it reduces the degree of node 7 from $k = 2$ to $k = 1$, node 7 is also removed, until there are no remaining nodes with a degree of 1. All the removed nodes (i.e., nodes 7, 8, and 9) and their linked edges form the 1-shell. The same operation will be repeated until all nodes in the graph have been assigned a shell.

In Sec. III-A1, the *DHC theorem* proved by Lü et al. [31] will be introduced, which establishes the relationship among degree, H-index, and coreness by generating a series of convergent sequences named H-indices for each node. Based on the DHC theorem, it is reasonable to assume that different networks have different convergence steps and each iteration of H-index sequences encodes information that can distinguish the network's properties. Methodologically, the *Shannon entropy* will be applied to extract and integrate information in these sequences, as further discussed below.

C. Shannon entropy

Without loss of generality, for a random variable X , suppose it has n possible values, and the probability corresponding to each value is p_i ($i = 1, 2, \dots, n$). Then, the Shannon entropy [33], [34] of the random variable X is defined as

$$H = - \sum_{i=1}^n p_i \log_2 p_i. \quad (\text{II.1})$$

It is well known that the wider the probability distribution of X , the greater X 's uncertainty is, and the higher its Shannon entropy will be.

As a result, Shannon entropy provides an intuitive and accurate metric for quantifying the amount of information contained in a random variable (or a system). Sec. III-A2 will illustrate how to apply the Shannon entropy to generate the whole graph embedding of a graph from its H-index sequences.

D. Whole graph embedding

The *whole graph embedding* [35] is a vector that can be generated by a learned mapping $\Phi : \mathcal{G} \rightarrow \mathbb{R}^k$, which maps a graph \mathcal{G} to the vector space \mathbb{R}^k , where k is the dimension of the vector. Whole graph embedding is supposed to capture the structural properties of a graph as much as possible. In practice, among different graphs, the ones with similar structural properties are supposed to be classified into the same category according to their whole graph embedding.

III. METHODS

In this section, DHC-entropy (DHC-E) is introduced in Sec. III-A and its performance on graph classification is evaluated in Sec. III-B.

A. DHC-entropy (DHC-E)

Since the information of nodal H-index sequences produced by the DHC theorem can be employed to represent and distinguish different graphs, the Shannon entropy is combined with the DHC theorem to develop a whole graph embedding method, called *DHC-entropy (DHC-E)*, which is explainable, extensible, and hyperparameter-free. In this section, the DHC theorem is reviewed in Sec. III-A1 and the Shannon entropy to the DHC-E is introduced in Sec. III-A2. Finally, the performance of DHC-E is compared to four state-of-the-art baselines in Sec. III-B using different evaluation metrics and datasets.

1) *DHC theorem*: The degree, H-index, and coreness all have advantages and disadvantages in measuring the influence of nodes in a graph. For instance, the degree and H-index are calculated based on the local topological information but cannot reflect the global characteristics of nodes in a graph. According to Kitsak et al. [36], the coreness is a better metric of nodal influence because it reflects global nodal location in a graph. However, calculating coreness is difficult and time-consuming on large-size graphs because it requires traversing global topological structures.

To address the problem, Lü et al. [31] proved the *DHC theorem*, which establishes the relationship among degree, H-index, and coreness. Methodologically, the H-index of a node in a graph can be calculated based on the degree centrality of its neighbors by using the method illustrated in Sec. II-B. Following that, the H-index of every node can be updated based on the previous H-indices of neighbors following the same procedure. This updating process will be continued iteratively, resulting in an H-index sequence for every node. The DHC theorem proves that each nodal H-index sequence eventually converges to the nodal coreness.

Mathematically, for a graph $G(V, E)$, the degree of an arbitrary node i is denoted by k_i and the degrees of its neighbors are $k_{j_1}, k_{j_2}, \dots, k_{j_{k_i}}$. Let operator \mathcal{H} represent the operation of calculating H-index. Then, the H-index of node i is defined as

$$h_i = \mathcal{H}(k_{j_1}, k_{j_2}, \dots, k_{j_{k_i}}). \quad (\text{III.1})$$

The $k_{j_1}, k_{j_2}, \dots, k_{j_{k_i}}$ are sorted by descending order. Denote the zero-order H-index and the first-order H-index in the H-index sequence of node i by k_i and h_i , respectively. Then, the n th-order H-index ($n > 0$) can be calculated by

$$h_i^{(n)} = \mathcal{H} \left(h_{j_1}^{(n-1)}, h_{j_2}^{(n-1)}, \dots, h_{j_{k_i}}^{(n-1)} \right), \quad (\text{III.2})$$

where $h_i^{(0)} = k_i, h_i^{(1)} = h_i$.

The DHC theorem proves that the H-index sequence $h_i^{(0)}, h_i^{(1)}, h_i^{(2)}, \dots$ of node i will converge to the node's core-ness c_i , i.e.,

$$c_i = \lim_{n \rightarrow \infty} h_i^{(n)}. \quad (\text{III.3})$$

The same is true for other nodes in $G(V, E)$. An example of the updating procedure is shown in Fig. 2.

In this way, the DHC theorem significantly reduces the computational complexity of computing nodal core-ness via establishing the convergence process from degree to core-ness and can be used for distributed computing to further improve computational performance.

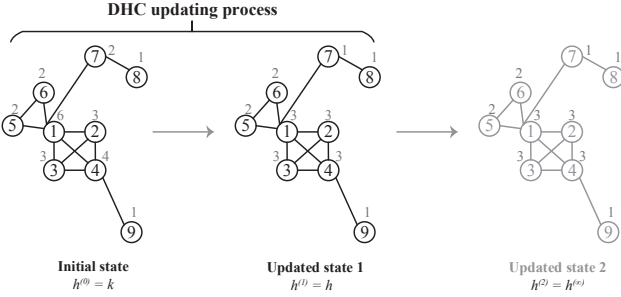


Fig. 2. **Schematics of DHC updating procedure.** The zero-order H-index of every node is initialized to its degree, as shown in the initial state. The following updated states can be calculated by the DHC theorem. When it comes to the updated state 2, the second-order H-index of each node is the same as that of the previous step (i.e., the first-order, $h^{(1)}$). So, the iterative update has already converged and the convergence values are the nodal core-ness, as shown in Fig. 1d.

2) *Combining Shannon entropy and DHC theorem:* Inspired by the idea of Weisfeiler-Lehman kernels [37] to represent a graph using the nodes' updated label information of each iteration within a convergence process, the *DHC-entropy* (DHC-E) is employed to leverage the information of H-index sequence of every node generated from the DHC updating process for the whole graph embedding. To achieve the goal, there are two critical issues to be solved: (1) How to extract and integrate the information generated from the DHC updating process (i.e., the H-index sequences of all nodes) to construct whole graph embedding; (2) How to unify and align the whole graph embedding with different dimensions.

As for the first problem, suppose there is a graph $G = (V, E)$ with n nodes (i.e., $|V| = n$), and the DHC updating process on the graph G converges after s iterations and generates n H-index sequences for all nodes as $\{h_1^{(0)}, h_1^{(1)}, h_1^{(2)}, \dots, h_1^{(s)}\}, \{h_2^{(0)}, h_2^{(1)}, h_2^{(2)}, \dots, h_2^{(s)}\}, \dots, \{h_n^{(0)}, h_n^{(1)}, h_n^{(2)}, \dots, h_n^{(s)}\}$. In an arbitrary iteration m ($0 \leq m \leq s$), the H-indices of all nodes, $h_1^{(m)}, h_2^{(m)}, \dots, h_n^{(m)}$, represent the graph's state at this iteration. DHC-E first calculates the probability distribution of $h_1^{(m)}, h_2^{(m)}, \dots, h_n^{(m)}$, and then

takes the probability distribution as the input to Formula (II.1) to calculate the Shannon entropy H_m , which quantifies the uncertainty of the graph in this state. Take the initial state in Fig. 2 as an example. Denote the H-index of a node as a random variable X . The probability distribution of H-indices in the initial state is $P(X = 6) = \frac{1}{9}, P(X = 3) = \frac{2}{9}, P(X = 4) = \frac{1}{9}, P(X = 2) = \frac{1}{3}, P(X = 1) = \frac{2}{9}$. Based on it, one can obtain the Shannon entropy of the initial state, $H_0 = \frac{1}{9} \log_2 \frac{1}{9} + \frac{2}{9} \log_2 \frac{2}{9} + \frac{1}{9} \log_2 \frac{1}{9} + \frac{1}{3} \log_2 \frac{1}{3} + \frac{2}{9} \log_2 \frac{2}{9} \approx 2.197$. The same is true for other states of the graph in different iterations. At the end of the DHC updating process, one obtains a Shannon entropy sequence of the graph G , as

$$(H_1, H_2, \dots, H_m, \dots, H_s),$$

where $H_m = \text{ShannonEntropy} \left(h_1^{(m)}, h_2^{(m)}, \dots, h_n^{(m)} \right),$ (III.4)

(H_1, H_2, \dots, H_m) is the whole graph embedding with m dimension of G in DHC-E.

When it comes to the second problem, given a set of graphs $\mathbb{G} = \{G_1, G_2, \dots\}$, their whole graph embeddings are supposed to be unified in dimension for downstream tasks such as graph classification. However, the DHC updating process for different graphs typically leads to whole graph embedding with unequal dimensions because the convergence steps of different graphs are usually nonuniform, as shown in Fig. 3 for example. In this case, the largest dimension among all the generated whole graph embeddings of \mathbb{G} will be taken as the unified baseline. Any embedding lower than this baseline in dimension will be expanded with its last element to be aligned. Compared with other dimension alignment strategies (e.g., using 0), expanding with the last element can ensure the whole graph embedding to maintain its unique features because the last element reflects the uncertainty of the graph's convergence state in the DHC updating process.

Overall, DHC-E is more explainable compared with other machine learning-based whole graph embedding methods. Intuitively, the DHC updating process of different graphs is distinctive in the convergence steps and gradients. To characterize the convergence process, instead of adopting the approach in Weisfeiler-Lehman kernels [37] to concatenate the label information of nodes directly, the uncertainty of the sequential states is taken into account in iterations. Shannon entropy is a powerful tool to use for this purpose.

B. Performance evaluation

The common task of graph classification is simulated to evaluate the performance of DHC-E, taking the embeddings produced from DHC-E as the input of the K-nearest neighbor (KNN) classifier, where the classification performance can be quantified by metrics Accuracy (ACC) and F1 score (F1). In order to explore the advantages and disadvantages of DHC-E compared with other graph representation models, the four state-of-the-art models illustrated in Sec. III-B4 are taken as baselines, implemented on the unified datasets described in Sec. III-B3.

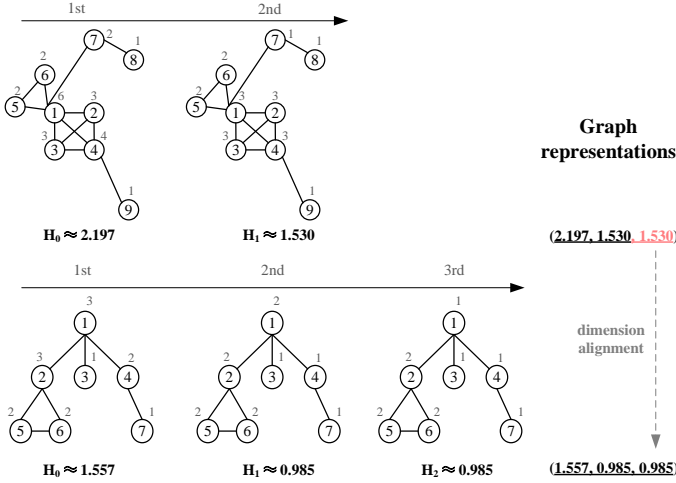


Fig. 3. **Schematics of DHC-E.** For the other states generated from the DHC updating process of a graph, the same rules are applied to calculate their Shannon entropy. At the end of the DHC updating process, one obtains two Shannon entropy sequences of the two graphs (2.197, 1.530) and (1.557, 0.985, 0.985), which are two graphs' embeddings. The two embeddings are with unequal dimensions. Based on the highest dimension of the two embeddings (i.e., 3), the last element of (2.197, 1.530) is used to expand (2.197, 1.530) to (2.197, 1.530, 1.530) for dimension alignment.

1) *Graph classification:* To assess the performance of DHC-E, the whole graph embedding as the input to the classifier for graph classification [38]. Specifically, given a set of graphs $\mathbb{G} = \{G_1, G_2, \dots, G_n\}$, $G_i = (V_i, E_i, l_i)$, where V_i and E_i denote the node set and edge set of G_i , respectively, and l_i is the label of G_i , where the graphs belonging to the same category have the same label l_i . By implementing DHC-E on each G_i in \mathbb{G} , n whole graph embedding are generated as

$$(H_{1,1}, \dots, H_{1,s_1}), \dots, (H_{i,1}, \dots, H_{i,s_i}), \dots, (H_{n,1}, \dots, H_{n,s_n}), \quad (\text{III.5})$$

where $H_{i,j}$ is the Shannon entropy of G_i calculated in the j -th iteration of the DHC updating process, and s_i is G_i 's convergence steps. The dimensions of the generated embedding are expanded to the same using the proposed dimension alignment method. By using these embedding, an $n \times s_{\max}$ matrix is built as

$$\begin{pmatrix} H_{1,1} & H_{1,2} & \dots & H_{1,s_1} & \dots & H_{1,s_1} \\ \dots & \dots & \dots & \dots & \dots & \dots \\ H_{i,1} & H_{i,2} & \dots & H_{i,s_i} & \dots & H_{i,s_i} \\ \dots & \dots & \dots & \dots & \dots & \dots \\ H_{n,1} & H_{n,2} & \dots & H_{n,s_n} & \dots & H_{n,s_n} \end{pmatrix}, \quad (\text{III.6})$$

where s_{\max} is the maximum convergence steps of the n graphs of \mathbb{G} in the DHC updating process. Finally, this matrix is used as the input to the K-nearest neighbor (KNN) classifier [39] for graph classification. Compared with other graph classification methods, such as support vector machine (SVM) [40], KNN is effective enough and more lightweight, which ensures the classification results be quickly and primarily determined by DHC-E. The pseudo code of DHC-E for graph classification is shown in Algorithm 1.

Algorithm 1. DHC-E for graph classification

Input: A set of n graphs $\mathbb{G} = \{G_1, G_2, \dots, G_n\}$, $G_i = (V_i, E_i, l_i)$.
Output: the classification results l'_1, l'_2, \dots, l'_n of \mathbb{G} .
1 : DHC_EntropyMatrix = [];
2 : for each $G_i = (V_i, E_i, l_i)$ in \mathbb{G} :
3 : $H_i = [d_1, d_2, \dots, d_{|V_i|}]$
4 : $H_{i,0} = \text{ShannonEntropy}(H_i)$
5 : $j=1$:
6 : while true:
7 : $H_i\text{Updated} = \text{DHC_UpdatingProcess}(H_i)$
8 : if $H_i\text{Updated}$ is equal to H_i :
9 : break
10 : else:
11 : $H_{i,j} = \text{ShannonEntropy}(H_i\text{Updated})$
12 : $H_i = H_i\text{Updated}$
13 : $j = j + 1$
14 : add $[H_{i,0}, H_{i,1}, \dots]$ to DHC_EntropyMatrix by row
15 : DHC_EntropyMatrix = DimensionAlignment(DHC_EntropyMatrix)
16 : $l'_1, l'_2, \dots, l'_n = \text{KNN}(\text{DHC_EntropyMatrix})$

Intuitively, the graphs that belong to the same category should have similar structural features, and vice versa. Whole graph embedding is supposed to capture and preserve these features as much as possible, which can classify graphs to their correct categories. Therefore, DHC-E is applied to graph classification tasks to assess its performance (i.e., whether it can generate accurate whole graph embedding to classify different graphs correctly).

2) *Evaluation metrics:* Accuracy (ACC) and F1 scores (F1) [41] are used to quantify the performance of graph classification results.

Let labels $L = (l_1, l_2, \dots, l_n)$ denote the categories of graphs in $\mathbb{G} = (G_1, G_2, \dots, G_n)$, $G_i = (V_i, E_i, l_i)$, respectively. Suppose the classification results of \mathbb{G} are $L' = (l'_1, l'_2, \dots, l'_n)$. Let TP (*True Positive*) denote the number of pair of graphs that belong to the same class in both L and L' , TN (*True Negative*) denote the number of pair of graphs that belong to the same class in L' but not in L , FP (*False Positive*) denote the number of pair of graphs that belong to the same class in L but not in L' , and FN (*False Negative*) denote the number of pair of graphs that do not belong to the same class in both L' and L .

ACC is defined as

$$\text{ACC} = \frac{TP + TN}{TP + TN + FP + FN}, \quad (\text{III.7})$$

F1 is defined as

$$\text{F1} = \frac{2 \times \text{precision} \times \text{recall}}{\text{precision} + \text{recall}}, \quad (\text{III.8})$$

where $\text{precision} = \frac{TP}{TP + FP}$ and $\text{recall} = \frac{TP}{TP + FN}$.

The better the performance of graph classification is, the larger the values of ACC and F1 will be.

3) *Datasets:* Several experimental datasets are used to extensively evaluate the performance of DHC-E, including *simulation datasets* and *real-world datasets*. **Simulation datasets** were constructed by generating a certain number of specific networks, including *random network (ER)* [42], *small-world network (SW)* [43], and *scale-free network (BA)* [44]. Each of them has unique structural characteristics and could be generated by specific algorithms, respectively. **Real-world datasets** were picked from online public resources-TUDataSets

[45] (<https://chrsmrrs.github.io/datasets/docs/datasets/>), used for graph classification. The simulation datasets were more convenient for use to explore the performance of DHC-E based on datasets with different complexity because one could control their node-scale and network's sparsity. Although this way led to different structures of ER, SW, and BA, their characteristics remain to be distinguishable from the other two categories. The real-world datasets directly evaluated the practical application value of DHC-E. This combination of simulated and real-world data allow for a more comprehensive evaluation of different models.

Besides, to evaluate the performance of the algorithm on intelligent biological systems, **Brain morphological similarity networks** were generated for autism spectrum disorders (ASD) and typical control (TC) participants, using the second iteration of Autism Brain Imaging Data Exchange (ABIDE II, http://fcon_1000.projects.nitrc.org/indi/abide/abide_II.html) [46]. The data were downloaded from the Indiana University site (ABIDE II). Forty participants were enrolled with 20 ASD and 20 TC participants. The ASD participants' age range is 17-54 years and TC's age range is 19-37 years. Computational Anatomy Toolbox (CAT 12, <http://www.neuro.uni-jena.de/cat/>) for SPM (<https://www.fil.ion.ucl.ac.uk/spm/software/spm12/>) was used to perform the surface analysis to calculate the cortical sulcal depth. Then, the data were resampled to a lower 32k mesh (average node spacing of ~ 2 mm) compatible with the Human Connectome Project (HCP) with a smoothing filter size of 25 mm. Specifically, to construct the brain network, nodes were first defined based on the Schaefer atlas [47] with 400 brain regions (*Schaefer2018_400Parcels_17Networks*). Second, the relationships among different nodes were calculated by the Earth Mover's Distance (EMD) (D_E) between the probability distribution function (PDF) of the brain cortical sulcal depth of any paired brain regions [48], [49]. In detail, the brain cortical sulcal depth value was extracted for each brain region. Then, the kernel density estimation (KDE) was used to estimate the probability density function of these sulcal depth values with 128 sampling points [28] for each brain region. The probability density function is standardized by dividing its sum to produce PDF for each brain region, and the EMD between the PDFs of any paired brain regions was used for constructing an EMD matrix (400×400). Subsequently, the EMD matrix was converted to a similarity matrix based on sigmoid function and termed the sulcal depth-based morphological similarity brain network M_{sim} , for each participant, as $M_{sim} = \sqrt{\frac{1}{1+D_E}}$. Finally, the M_{sim} was thresholded into a binary network by keeping the top 10% edges. Fig. 4 shows the details.

Datasets for binary classification. SW and BA were used to construct simulation datasets with distinctive complexity named *categorized datasets by simulation*, as shown in Table. VI. For real-world datasets, selected from online public resources-TUDatasets [45] (<https://chrsmrrs.github.io/datasets/docs/datasets/>), where each one corresponded to a specific application domain such as social network or biology information network, they were classified into multiple subcategories, named *sub-categorized datasets from the real world*, as shown

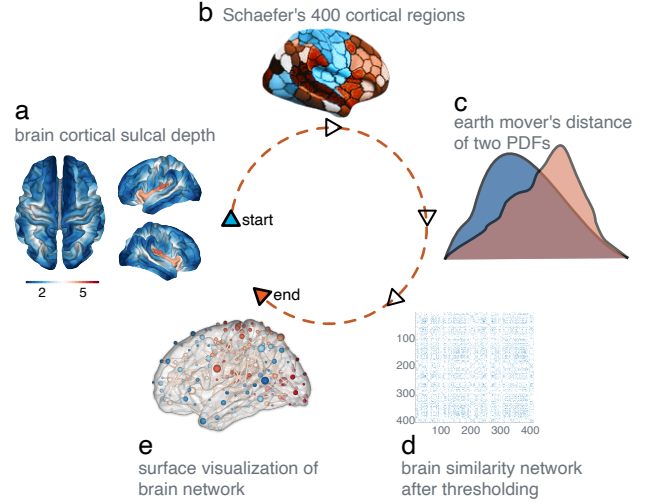


Fig. 4. **Flowchart of constructing the brain sulcal depth similarity network.** **a**, First obtain the sulcal depth for each node in the brain surface space. **b**, Then, use the Schaefer 400 atlas to define the brain nodes. **c**, For each brain region, estimate their PDF of sulcal depth and calculate the earth mover's distance between any paired brain regions, resulting in a 400×400 similarity matrix with top 10% edges preserved (**d**), Convert the distance metric to similarity metric through sigmoid function. **e**, Plot the surface of the brain sulcal depth similarity network.

in Table. VII. To further explore the performance of DHC-E in classifying networks that belong to different domains, the above datasets were combined to construct compound ones, named *categorized datasets*, as shown in Table. VIII.

Datasets for multi-class classification. Multi-class classification has become increasingly important in recent years, which were tested because the diversity of application situations of an algorithm also determines its generalization and value. The construction of datasets is the same as that of the datasets used for binary classification, where the only difference is that the categories of datasets for multi-class classification are more diverse, as shown in Tabs. IX, X, and XI.

4) *Baselines*: The four baselines introduced in Sec. I, including the Graph2vec, Invariant Graph Embedding (IGE), Graph and Line Graph to Vector (GL2vec), and Network Laplacian Spectral Descriptor (NetLSD), were used to evaluate DHC-E and analyze its pros and cons in different classification tasks.

To ensure the fairness of performance comparison, the embeddings obtained from different models were taken as the input of a common KNN model with fixed hyperparameters for graph classification (i.e., line 16 in Algorithm 1). Based on the split strategy of 90% training samples and 10% test samples at random, the implementation of the KNN classifier was repeated 500 times with 10-repeated and 10-fold cross-validation for each model to obtain their overall performance.

IV. EXPERIMENTAL RESULTS

The results of ACC and F1 for DHC-E, as well as for the baselines on multiple datasets for binary and multi-class classification tasks, are described in Fig. 5, Table. I and Table. II, respectively. The stability and time complexity of

DHC-E and baselines on these datasets are also assessed and presented in Table. III and Table. IV, respectively. Overall, the proposed DHC-E model obtains a second rank across all the datasets based on the mean classification value. Furthermore, DHC-E obtains a trade-off among the accuracy, stability, and time complexity. Besides, to explore the extensibility of DHC-E on brain network, it was combined with baselines and then the performance of the combined models was evaluated, with results shown in Table.V. Furthermore, an application of DHC-E on graph visualization is shown in Fig. 6.

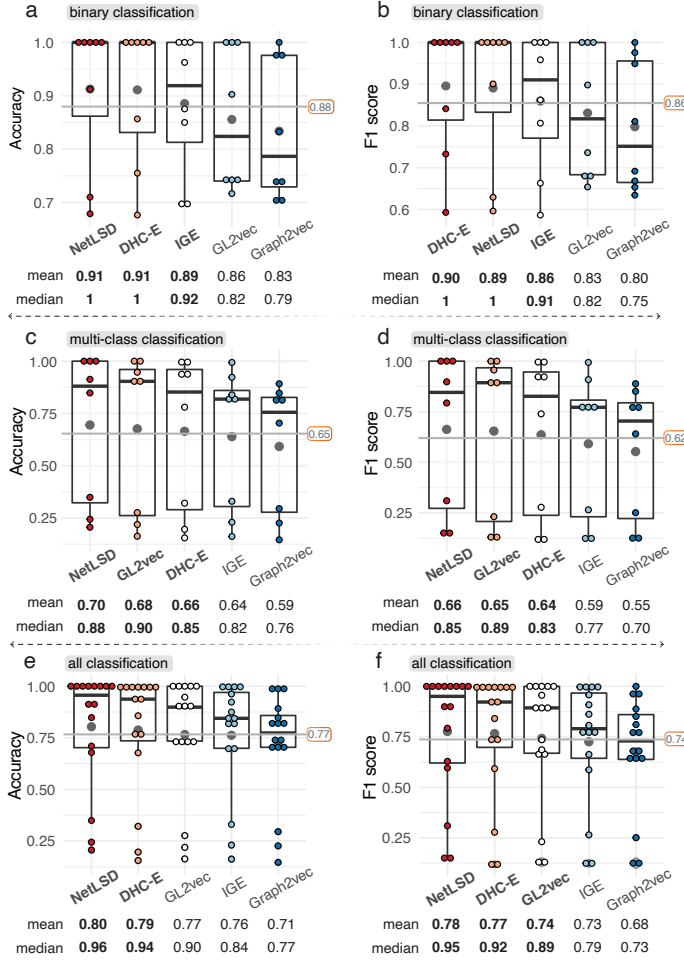


Fig. 5. **Classification performance of different graph embedding models.** The plots were sorted by their mean values (in descending order). For binary classification (B1-B8), the accuracy and F1 score is presented in **a** and **b**, respectively. For multi-class classification (M1-M8), the accuracy and F1 score is presented in **c** and **d**, respectively. For all cases (B1-B8 and M1-M8), the accuracy and F1 score is presented in **e** and **f**, respectively. The black dots indicate the mean classification value of each model, and the gray lines indicate the mean classification value across all models.

A. Results on binary graph classification

For binary graph classification, the ACC and F1 results for DHC-E and baselines are summarized in Table. I, in which the eight datasets are classified into three different subtasks for binary graph classification (i.e., the subtasks based on *categorized datasets by simulation*, *sub-categorized datasets from the real world*, and *categorized datasets*), where the ACC and F1 results for evaluated methods are averaged, respectively. The hyperparameter settings of baselines follow the default values in the python package, named *karate club*, as shown in Table. XII. Each result is calculated by averaging over 500 runs with independently random split train-test sets. The top three results with the highest ACC and F1 on the three subtasks are respectively emphasized in strong yellow color. It shows that the overall advantages of DHC-E are still satisfactory on the three subtasks compared with that of baselines, but not as prominent as that on binary graph classification tasks.

Specifically, on the first subtask (i.e., M1, M2, and M3), although DHC-E is 1.36 % and 1.90% lower than both NetLSD and GL2vec over ACC and F1, respectively, it still significantly outperforms IGE and Graph2vec, where the ACC and F1 results of DHC-E are 12.3% and 15.9% higher than

from the real world, and categorized datasets), where the ACC and F1 results for evaluated models are averaged, respectively. The hyperparameter settings of baselines follow the default values in the python package, named *karate club*, as shown in Table. XII. Each result is calculated by averaging over 500 runs on independently random split train-test sets. The top three results with the highest ACC and F1 on the three subtasks are respectively emphasized in strong yellow color. Clearly, DHC-E outperforms other models overall in terms of F1 on all three subtasks. As for ACC, except for the second subtask where NetLSD performs slightly better than DHC-E, for which DHC-E still achieves good performance.

From the averaged performance of evaluated models on the three subtasks, DHC-E achieved the best the overall accuracy on the third subtask (i.e., B7 and B8), followed by the first subtask (i.e., B1, B2, and B3), and finally the second subtask (i.e., B4, B5, and B6). Specifically, in comparing the overall performance of DHC-E with the weakest baseline on the three subtasks, DHC-E outperforms Graph2vec on the first subtask (i.e., B1, B2, and B3) by 16.6% and 22.7% over ACC and F1, respectively. When it comes to the second subtask (B4, B5, and B6), the ACC and F1 results of DHC-E are 6.7% and 7.6% higher than those of Graph2vec, respectively. Similarly, on the third task (i.e., B7 and B8) DHC-E outperforms GL2vec by 5.2% and 5.4% over ACC and F1, respectively. Clearly, the advantages of DHC-E over other baselines are distinctive in different subtasks, which are smaller on the first and third subtasks than that on the second subtask.

These results indicate that the difficulty of graph sets to be classified may be distinctive under specific scenarios. Thus, one should make a trade-off between accuracy and stability (see Table. III), and time consuming (see Table. IV), in order to select appropriate models for graph classification.

B. Results on multi-class graph classification

For multi-class graph classification tasks, the ACC and F1 results for DHC-E and baselines are summarized in Table. II, in which the eight datasets are classified into three different subtasks for multi-class graph classification (i.e., the subtasks based on *categorized datasets by simulation*, *sub-categorized datasets from the real world*, and *categorized datasets*), where the ACC and F1 results for evaluated methods are averaged, respectively. The hyperparameter settings of baselines follow the default values in the python package, named *karate club*, as shown in Table. XII. Each result is calculated by averaging over 500 runs with independently random split train-test sets. The top three results with the highest ACC and F1 on the three subtasks are respectively emphasized in strong yellow color. It shows that the overall advantages of DHC-E are still satisfactory on the three subtasks compared with that of baselines, but not as prominent as that on binary graph classification tasks.

Specifically, on the first subtask (i.e., M1, M2, and M3), although DHC-E is 1.36 % and 1.90% lower than both NetLSD and GL2vec over ACC and F1, respectively, it still significantly outperforms IGE and Graph2vec, where the ACC and F1 results of DHC-E are 12.3% and 15.9% higher than

TABLE I
RESULTS ON BINARY GRAPH CLASSIFICATION TASKS.

datasets	DHC-E		Graph2vec		IGE		GL2vec		NetLSD	
	ACC	F1	ACC	F1	ACC	F1	ACC	F1	ACC	F1
B1	1.000	1.000	1.000	1.000	0.850	0.807	0.740	0.674	1.000	1.000
B2	1.000	1.000	0.740	0.634	1.000	1.000	1.000	1.000	1.000	1.000
B3	1.000	1.000	0.833	0.811	0.962	0.958	1.000	1.000	1.000	1.000
Avg.	1.000	1.000	0.858	0.815	0.937	0.922	0.913	0.891	1.000	1.000
B4	0.857	0.841	0.704	0.692	0.875	0.862	0.745	0.736	0.912	0.901
B5	0.755	0.733	0.704	0.668	0.701	0.663	0.717	0.686	0.679	0.629
B6	0.677	0.593	0.738	0.653	0.694	0.587	0.740	0.654	0.710	0.596
Avg.	0.763	0.722	0.715	0.671	0.757	0.704	0.734	0.692	0.767	0.709
B7	1.000	1.000	0.977	0.976	1.000	1.000	0.903	0.898	1.000	1.000
B8	1.000	1.000	0.975	0.949	1.000	1.000	1.000	1.000	1.000	1.000
Avg.	1.000	1.000	0.976	0.962	1.000	1.000	0.951	0.949	1.000	1.000

those of IGE, and 23.3% and 30.2% higher than those of Graph2vec, respectively. As for the second subtask (i.e., M4, M5, and M6), DHC-E achieves the accuracy in the middle level among all models. On the third subtask (i.e., M7 and M8), DHC-E is slightly inferior in the evaluated models. Its ACC and F1 results are 4.4% and 3.6 % lower than that of the best-performed baseline (i.e., NetLSD), respectively.

Besides, it is clear that the overall accuracy of all models on the second subtask (i.e., M4, M5, and M6) is much worse compared with that on the other two subtasks, as shown in Table. II. This result reveals that the research of methods for multi-class classification remains to be a great challenge today.

C. Stability analysis

Stability, opposed to deviation from averaged performance of a model, is also an important metric for assessment, for it quantifies the potential of a model to reach its best performance compared with baselines, which determines the cost of experiments.

The corresponding standard deviations of the ACC and F1 results for DHC-E and baselines on datasets for both binary classification and multi-class classification are summarized in Table. III, in which each value is the standard deviation corresponding to ACC or F1 in Tabs. I and II, which reveals the stability of different methods over 500 runs with independently random split train-test sets. The top three averaged results with the lowest standard deviation are emphasized in strong yellow color. For a model, the lower the averaged standard deviations of ACC and F1 results, the higher the model’s stability. As shown in Table. III, DHC-E has satisfactory stability among the evaluated models.

Taking both the accuracy and the stability of models into account provides a more comprehensive assessment of their performance. For example, although DHC-E has 4.1% and 6.6% lower averaged ACC and F1 (i.e., accuracy) than GL2vec on the datasets M7 and M8 (see Table. II), it nevertheless has 71.4% and 50% lower averaged standard deviation than GL2vec over ACC and F1, respectively, as shown in Table. III, which indicates that DHC-E is far more stable than GL2vec.

D. Time complexity analysis

In practice, the time complexity of models is an essential factor to be assessed because high accurate models with burdensome time complexity will also be of little significance and advantage, especially on large-scale datasets. Therefore, the time complexity of DHC-E and baselines were evaluated in order to make a more comprehensive trade-off between accuracy and complexity.

The corresponding consuming time of DHC-E and baselines on datasets for binary classification and multi-class classification is summarized in Table. IV, in which the results of consuming time are averaged from 500 separate runs, and the time is measured in seconds. The top three averaging results with the shortest consumption time are highlighted in strong yellow color. The results of DHC-E having the shortest consuming time on some datasets are also highlighted in strong yellow color. All experiments are implemented using Python 3.8 on a cluster server produced by AMAX equipped with four Intel Core E7-4820 V4 central processing units (CPU) operating at 2.00GHz and 1024GB of random access memory (RAM). For the sake of simplicity, the consuming time spent on tuning parameters for the models with hyperparameters (i.e., Graph2vec, IGE, GL2vec, and NetLSD) is not taken into account. As shown in Table. IV, although DHC-E is slower than most baselines overall, its time complexity is still acceptable. Meanwhile, the averaged consuming time of DHC-E is 180.3% lower than GL2vec, which indicates that machine learning-based graph embedding methods are not always faster than DHC-E.

More specifically, in some small-scale datasets like B4, B5, M4, and M6, DHC-E outperforms baselines. However, with the increase of data scale, the disadvantage of DHC-E in time complexity compared with baselines becomes more prominent, especially on B6, B8, and M8. These results demonstrate pros and cons between DHC-E and baselines. On the one hand, for binary classification tasks, DHC-E can achieve optimal overall performance. In that case, DHC-E can be preferred on small-scale datasets. If experimental equipments allow, DHC-E is also recommended for larger-scale datasets. On the other hand, for multi-class classification tasks, the criterion for model

TABLE II
RESULTS ON MULTI-CLASS GRAPH CLASSIFICATION TASKS.

datasets	DHC-E		Graph2vec		IGE		GL2vec		NetLSD	
	ACC	F1	ACC	F1	ACC	F1	ACC	F1	ACC	F1
M1	1.000	1.000	0.820	0.775	0.827	0.771	1.000	1.000	1.000	1.000
M2	0.950	0.932	0.704	0.640	0.923	0.909	1.000	1.000	1.000	1.000
M3	0.925	0.913	0.807	0.768	0.810	0.774	0.913	0.898	0.913	0.898
Avg.	0.958	0.948	0.777	0.728	0.853	0.818	0.971	0.966	0.971	0.966
M4	0.321	0.278	0.295	0.251	0.330	0.265	0.276	0.231	0.349	0.310
M5	0.155	0.119	0.146	0.114	0.162	0.120	0.163	0.124	0.206	0.159
M6	0.196	0.119	0.226	0.136	0.230	0.128	0.219	0.136	0.244	0.141
Avg.	0.224	0.172	0.222	0.167	0.241	0.171	0.219	0.164	0.266	0.204
M7	0.991	0.991	0.892	0.888	0.994	0.994	0.894	0.889	1.000	1.000
M8	0.780	0.740	0.847	0.851	0.839	0.773	0.947	0.956	0.848	0.793
Avg.	0.885	0.866	0.870	0.870	0.916	0.883	0.921	0.923	0.924	0.897

TABLE III
STABILITY ANALYSIS.

datasets	DHC-E		Graph2vec		IGE		GL2vec		NetLSD	
	ACC	F1	ACC	F1	ACC	F1	ACC	F1	ACC	F1
B1	0.000	0.000	0.000	0.000	0.000	0.000	0.032	0.036	0.000	0.000
B2	0.000	0.000	0.028	0.033	0.000	0.000	0.000	0.000	0.000	0.000
B3	0.000	0.000	0.029	0.036	0.000	0.000	0.000	0.000	0.000	0.000
B4	0.011	0.012	0.012	0.012	0.003	0.004	0.018	0.018	0.006	0.007
B5	0.014	0.015	0.031	0.039	0.000	0.000	0.030	0.037	0.000	0.000
B6	0.031	0.036	0.054	0.073	0.057	0.079	0.000	0.000	0.000	0.000
B7	0.000	0.000	0.005	0.005	0.000	0.000	0.011	0.012	0.000	0.000
B8	0.000	0.000	0.006	0.014	0.000	0.000	0.000	0.000	0.000	0.000
M1	0.000	0.000	0.000	0.000	0.000	0.000	0.000	0.000	0.000	0.000
M2	0.012	0.018	0.059	0.067	0.000	0.000	0.000	0.000	0.000	0.000
M3	0.010	0.012	0.026	0.031	0.000	0.000	0.001	0.001	0.000	0.000
M4	0.013	0.013	0.030	0.028	0.000	0.000	0.029	0.026	0.000	0.000
M5	0.007	0.006	0.015	0.013	0.000	0.000	0.014	0.012	0.000	0.000
M6	0.011	0.008	0.025	0.019	0.000	0.000	0.024	0.019	0.000	0.000
M7	0.002	0.002	0.010	0.011	0.000	0.000	0.011	0.012	0.000	0.000
M8	0.005	0.003	0.009	0.010	0.000	0.000	0.006	0.005	0.000	0.000
Avg.	0.007	0.008	0.021	0.024	0.004	0.005	0.011	0.011	$< 10^{-6}$	$< 10^{-6}$

selection depends on whether it needs to be hyperparameter-free because tuning hyperparameters for optimal performance of models may take a considerable amount of extra time.

E. Extensibility analysis of DHC-E on brain network

To evaluate the extensibility of DHC-E, DHC-E was integrated with the four baselines as *Graph2vec+DHC-E*, *IGE+DHC-E*, *GL2vec+DHC-E*, and *NetLSD+DHC-E*, respectively, by means of concatenating the embeddings obtained from DHC-E and baselines, normalized by Z-score for each model [50]. Subsequently, the accuracy of these extended models were evaluated by the brain dataset (B6), as shown in Table. V, where "+" denotes a combination of a baseline model and DHC-E. For each combination, the upper row represents the ACC and F1 results of the baseline model and their corresponding standard deviations in parentheses, and the lower row represents the same results of the baseline model combined with DHC-E. The best results before and after the combination with DHC-E are emphasized in strong yellow color for every baseline. Clearly, after integrating DHC-E with

baselines, the stability of baselines is improved. Furthermore, the ACC and F1 results of IGE on B6 are significantly enhanced by 10.4% and 17.7%, respectively, which achieves the best performance on B6 compared with the evaluated models before integrating with DHC-E. These results indicate that DHC-E has good extensibility and may help other embedding models break through their performance ceiling on graph classification within acceptable computational complexity.

F. Graphs visualization with DHC-E features

Visualizing each graph individually cannot effectively characterize the relationships among graphs, and if these graphs are put together, it will be miscellaneous. However, if we can effectively embed the different graphs into a two-dimensional space, the technique will have direct applications in industry and big data screen display. Therefore, we conducted an exploratory analysis in graph visualization applications to verify whether the DHC-E embedding method can adequately express different graphs in a two-dimensional space. First, we generated 20 small-world networks, 20 BA networks, and 20

TABLE IV
TIME COMPLEXITY ANALYSIS.

datasets	Time (DHC-E)	Time (Graph2vec)	Time (IGE)	Time (GL2vec)	Time (NetLSD)
B1	5.002	2.280	3.378	3.461	3.266
B2	7.740	2.668	7.317	69.491	5.134
B3	28.675	3.866	42.268	636.969	16.718
B4	3.698	6.518	13.048	10.688	15.703
B5	7.551	10.569	16.902	13.385	9.619
B6	176.177	3.351	50.065	495.777	28.012
B7	8.140	6.792	14.966	17.311	14.734
B8	181.634	7.940	67.482	473.768	20.710
M1	6.688	2.466	4.840	4.506	2.859
M2	9.077	3.359	10.619	191.478	4.201
M3	37.320	6.543	70.885	807.907	3.905
M4	6.246	11.068	18.957	9.934	10.537
M5	96.563	7.398	31.545	23.254	16.197
M6	6.027	10.825	17.899	10.081	10.675
M7	10.285	8.386	25.682	10.549	11.104
M8	266.728	23.503	101.683	444.753	31.876
Avg.	53.597	7.346	31.096	201.457	12.828

TABLE V
RESULTS OF BASELINES AND THEIR COMBINATIONS WITH DHC-E ON THE BRAIN DATASET B6.

	ACC	F1
Graph2vec	0.738 (0.054)	0.653 (0.073)
+DHC-E	0.734 (0.020)	0.649 (0.026)
IGE	0.694 (0.057)	0.587 (0.079)
+DHC-E	0.766 (0.022)	0.691 (0.028)
GL2vec	0.740 ($< 10^{-6}$)	0.654 ($< 10^{-6}$)
+DHC-E	0.715 ($< 10^{-6}$)	0.617 ($< 10^{-6}$)
NetLSD	0.710 ($< 10^{-6}$)	0.596 ($< 10^{-6}$)
+DHC-E	0.725 ($< 10^{-6}$)	0.626 ($< 10^{-6}$)

random networks. Then, we combined these 60 networks with 20 ASD brain networks into a new dataset. To that end, we performed the DHC-E analysis on these 80 graphs and obtained whole graph embedding for each graph. Subsequently, we performed principal component analysis (PCA) [9] on the obtained embedded features to further reduce the embedding features to two dimensions. We observed that the first two PCs explain about 99.6% of the total variability for whole graph embedding. Finally, we plotted the four categories of networks in a two-dimensional space composed of pc1 and pc2, where we found that it can cluster together graphs in the same category, which show the potential applications of DHC-E in lower-dimensional morphospace representation of graphs, as illustrated by Fig. 6 in details.

V. CONCLUSION

We developed a simple, hyperparameter-free, extensible, and explainable graph embedding method and evaluate its performance on classification tasks using different datasets. Through extensive experiments, we found that our model is comparable but straightforward to current sophisticated graph embedding methods. Our solution avoids such problems as choosing suitable hyperparameters and weak interpretability. Our results show that simple models can be competitive with-

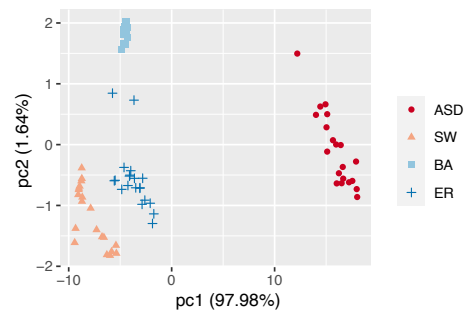


Fig. 6. Lower-dimension morphospace representation of graph with DHC-E features, we use the PCA to reduce the DHC-E whole graph embedding features into a two-dimension space and find that the DHC-E features can cluster together graphs in the same category. ASD, autism spectrum disorders’ brain network; SW, small-world network; BA, scale-free network; ER, random network.

out the need of choosing parameters. As it stands, our whole graph embedding method may be helpful for further designing simple-effective models. Additionally, our model shows good extensibility on brain networks with promising potential in lower-dimensional graph visualization. Future work involves more datasets and graph embedding methods for evaluating the performance in graph classification, graph visualization, and image classification. Conversely, brain disorders prediction will provide more insights and better understanding for studying new simple and powerful graph embedding methods.

APPENDIX A EXPERIMENTAL DATASETS AND HYPERPARAMETERS OF EXPERIMENTAL BASELINES

TABLE VI
DESCRIPTION OF SIMULATION DATASETS FOR BINARY CLASSIFICATION.

datasets	Sample size	Node-scale configuration	Sparsity configuration	Total size
B1	10	[100]	[0.1]	$2 \times 10 \times 1 = 20$
B2	10	[100]	[0.1, 0.9]	$2 \times 10 \times 2 = 40$
B3	10	[100, 200]	[0.1, 0.9]	$2 \times 10 \times 4 = 80$

For example, the node-scale configuration and sparsity configuration of B3 is [100, 200] and [0.1, 0.9], which indicates that it has four possible configurations (i.e., [100, 0.1], [100, 0.9], [200, 0.1], [200, 0.9]) for each category of the generated networks. Since there are ten samples for each category, the total sample size will be generated for each category of networks under the four configurations, which is 40. There are two categories of networks (i.e., SW and BA), so the size of B3 is $2 \times 10 \times 4 = 80$.

TABLE VII
DESCRIPTION OF REAL-WORLD DATASETS IN SPECIFIC DOMAINS FOR BINARY CLASSIFICATION.

datasets	Name	Graphs	Categories	Avg. nodes	Avg. edges	Domain
B4	MUTAG	188	2	17.93	19.79	small molecules
B5	highschool_ct1	180	2	52.32	544.81	social networks
B6	bin_sulc	40	2	400	15960	brain networks

Each comes from a specific domain and is further subdivided into different categories that belong to this domain. For instance, B4 is a dataset about small molecules named MUTAG. It contains 188 graphs with two categories, and the average nodes and average edges are 17.93 and 19.97, respectively.

TABLE VIII
DESCRIPTION OF COMBINATIONS DATASETS FOR BINARY CLASSIFICATION.

datasets	Combinations
B7	B4, B5
B8	B5, B6

For instance, B4 and B5 are combined together to construct B7 for binary graph classification. The graphs in B4 are unified into one category (i.e., small molecules), and those in B5 belong to another (i.e., social networks).

TABLE IX
DESCRIPTION OF SIMULATION DATASETS FOR MULTI-CLASS CLASSIFICATION.

datasets	Sample size	Node-scale configuration	Sparsity configuration	Total size
M1	10	[100]	[0.1]	$3 \times 10 \times 1 = 30$
M2	10	[100]	[0.1, 0.9]	$3 \times 10 \times 2 = 60$
M3	10	[100, 200]	[0.1, 0.9]	$3 \times 10 \times 4 = 120$

ER, SW, and BA are used to construct simulation datasets for multi-class classification.

TABLE X
DESCRIPTION OF REAL-WORLD DATASETS IN SPECIFIC DOMAINS FOR MULTI-CLASS CLASSIFICATION.

datasets	Name	Graphs	Categories	Avg. nodes	Avg. edges	Domain
M4	MSRC_9	221	8	40.58	97.94	computer vision
M5	MSRC_21	563	20	77.52	198.32	computer vision
M6	MSRC_21C	209	20	40.28	96.60	computer vision

Computer vision is a popular application domain of multi-class graph classification.

TABLE XI
DESCRIPTION OF COMBINATIONS DATASETS FOR MULTI-CLASS CLASSIFICATION.

datasets	Combinations
M7	B4, B5, M4
M8	B4, B5, B6, M4, M5, M6

Within M8, M4-M6 are unified into the same category because the graphs therein come from the computer vision domain. Thus, M8 has four categories.

TABLE XII
HYPERPARAMETERS OF BASELINES.

Models	hyperparameters
DHC-E	none
Graph2vec	wl_iterations = 2, dimension = 128, epochs = 10, learning_rate = 0.025, down_sampling = 0.0001, min_count = 5, seed = 42
IGE	feature_embedding_dimensions = [3,5], spectral_embedding_dimensions = [10,20], histogram_bins = [10,20], seed = 42
GL2vec	wl_iterations = 2, dimension = 128, epoches = 10, learning_rate = 0.025, down_sampling = 0.0001, min_count = 5, seed = 42
NetLSD	scale_min = -2.0, scale_max = 2.0, scale_steps = 250, approximation = 200, seed = 42

The hyperparameters of baselines adopted in experiments follow the default values in the python package named *karate club*. Distinctively, DHC-E requires zero hyperparameters for its implementation.

REFERENCES

- [1] K. Oono and T. Suzuki, "Graph neural networks exponentially lose expressive power for node classification," *arXiv: Learning*, 2020.
- [2] F. Nie, W. Zhu, and X. Li, "Unsupervised large graph embedding," in *Proceedings of the AAAI Conference on Artificial Intelligence*, vol. 31, no. 1, 2017.
- [3] M. Jacomy, T. Venturini, S. Heymann, and M. Bastian, "Forceatlas2, a continuous graph layout algorithm for handy network visualization designed for the gephi software," *PLoS One*, vol. 9, no. 6, p. e98679, 2014.
- [4] V. Menon, "Large-scale brain networks and psychopathology: a unifying triple network model," *Trends in Cognitive Sciences*, vol. 15, pp. 483–506, 2011.
- [5] A. Barabási, "Scale-free networks: A decade and beyond," *Science*, vol. 325, pp. 412 – 413, 2009.
- [6] B. Perozzi, R. Al-Rfou, and S. Skiena, "Deepwalk: Online learning of social representations," in *Proceedings of the 20th ACM SIGKDD International Conference on Knowledge Discovery and Data Mining*, 2014, pp. 701–710.
- [7] A. Grover and J. Leskovec, "node2vec: Scalable feature learning for networks," in *Proceedings of the 22nd ACM SIGKDD International Conference on Knowledge Discovery and Data Mining*, 2016, pp. 855–864.
- [8] P. Velickovic, G. Cucurull, A. Casanova, A. Romero, P. Lio, and Y. Bengio, "Graph attention networks," *ArXiv*, vol. abs/1710.10903, 2018.
- [9] S. Wold, K. Esbensen, and P. Geladi, "Principal component analysis," *Chemometrics and Intelligent Laboratory Systems*, vol. 2, pp. 37–52, 1987.
- [10] S. Balakrishnama and A. Ganapathiraju, "Linear discriminant analysis—a brief tutorial," *Institute for Signal and Information Processing*, vol. 18, no. 1998, pp. 1–8, 1998.
- [11] J. Kruskal, "Multidimensional scaling by optimizing goodness of fit to a nonmetric hypothesis," *Psychometrika*, vol. 29, pp. 1–27, 1964.

- [12] J. Tenenbaum, "The isomap algorithm and topological stability," *Science*, vol. 295, pp. 9–9, 2002.
- [13] M. Belkin and P. Niyogi, "Laplacian eigenmaps for dimensionality reduction and data representation," *Neural Computation*, vol. 15, pp. 1373–1396, 2003.
- [14] T. Mikolov, I. Sutskever, K. Chen, G. S. Corrado, and J. Dean, "Distributed representations of words and phrases and their compositionality," in *Advances in Neural Information Processing Systems*, 2013, pp. 3111–3119.
- [15] T. Mikolov, K. Chen, G. Corrado, and J. Dean, "Efficient estimation of word representations in vector space," *arXiv preprint arXiv:1301.3781*, 2013.
- [16] S. Cao, W. Lu, and Q. Xu, "Grarep: Learning graph representations with global structural information," in *Proceedings of the 24th ACM International Conference on Information and Knowledge Management*, 2015, pp. 891–900.
- [17] A. Bordes, N. Usunier, A. Garcia-Duran, J. Weston, and O. Yakhnenko, "Translating embeddings for modeling multi-relational data," in *Advances in Neural Information Processing Systems*, 2013, pp. 2787–2795.
- [18] P. Yanardag and S. Vishwanathan, "Deep graph kernels," in *Proceedings of the 21th ACM SIGKDD International Conference on Knowledge Discovery and Data Mining*, 2015, pp. 1365–1374.
- [19] A. Narayanan, M. Chandramohan, R. Venkatesan, L. Chen, Y. Liu, and S. Jaiswal, "graph2vec: Learning distributed representations of graphs," *arXiv preprint arXiv:1707.05005*, 2017.
- [20] S. Verma and Z.-L. Zhang, "Hunt for the unique, stable, sparse and fast feature learning on graphs," in *Proceedings of the 31st International Conference on Neural Information Processing Systems*, 2017, pp. 87–97.
- [21] A. Tsitsulin, D. Mottin, P. Karras, A. Bronstein, and E. Müller, "Netlsd: Hearing the shape of a graph," *Proceedings of the 24th ACM SIGKDD International Conference on Knowledge Discovery & Data Mining*, 2018.
- [22] A. Galland and M. Lelarge, "Invariant embedding for graph classification," in *ICML 2019 Workshop on Learning and Reasoning with Graph-Structured Data*, 2019.
- [23] H. Chen and H. Koga, "G12vec: Graph embedding enriched by line graphs with edge features," in *International Conference on Neural Information Processing*. Springer, 2019, pp. 3–14.
- [24] D. B. West *et al.*, *Introduction to graph theory*. Prentice Hall Upper Saddle River, 2001, vol. 2.
- [25] S. Pei and H. A. Makse, "Spreading dynamics in complex networks," *Journal of Statistical Mechanics: Theory and Experiment*, vol. 2013, no. 12, p. P12002, 2013.
- [26] E. Muller and R. Peres, "The effect of social networks structure on innovation performance: A review and directions for research," *International Journal of Research in Marketing*, vol. 36, no. 1, pp. 3–19, 2019.
- [27] O. Sporns, C. J. Honey, and R. Kötter, "Identification and classification of hubs in brain networks," *PloS One*, vol. 2, no. 10, p. e1049, 2007.
- [28] H. Wang, X. Jin, Y. Zhang, and J. Wang, "Single-subject morphological brain networks: connectivity mapping, topological characterization and test-retest reliability," *Brain Behav*, vol. 6, no. 4, p. e00448, 2016.
- [29] L. Lü, D. Chen, X.-L. Ren, Q.-M. Zhang, Y.-C. Zhang, and T. Zhou, "Vital nodes identification in complex networks," *Physics Reports*, vol. 650, pp. 1–63, 2016.
- [30] J. E. Hirsch, "An index to quantify an individual's scientific research output," *Proceedings of the National academy of Sciences*, vol. 102, no. 46, pp. 16 569–16 572, 2005.
- [31] L. Lü, T. Zhou, Q.-M. Zhang, and H. E. Stanley, "The h-index of a network node and its relation to degree and coreness," *Nature Communications*, vol. 7, no. 1, pp. 1–7, 2016.
- [32] S. N. Dorogovtsev, A. V. Goltsev, and J. F. F. Mendes, "K-core organization of complex networks," *Physical Review Letters*, vol. 96, no. 4, p. 040601, 2006.
- [33] P. Bromiley, N. Thacker, and E. Bouhova-Thacker, "Shannon entropy, renyi entropy, and information," *Statistics and Inf. Series (2004-004)*, 2004.
- [34] C. E. Shannon, "A mathematical theory of communication," *The Bell System Technical Journal*, vol. 27, no. 3, pp. 379–423, 1948.
- [35] D. Zhang, J. Yin, X. Zhu, and C. Zhang, "Network representation learning: A survey," *IEEE transactions on Big Data*, vol. 6, no. 1, pp. 3–28, 2018.
- [36] M. Kitsak, L. K. Gallos, S. Havlin, F. Liljeros, L. Muchnik, H. E. Stanley, and H. A. Makse, "Identification of influential spreaders in complex networks," *Nature Physics*, vol. 6, no. 11, pp. 888–893, 2010.
- [37] N. Shervashidze, P. Schweitzer, E. J. Van Leeuwen, K. Mehlhorn, and K. M. Borgwardt, "Weisfeiler-lehman graph kernels," *Journal of Machine Learning Research*, vol. 12, no. 9, 2011.
- [38] N. M. Kriege, F. D. Johansson, and C. Morris, "A survey on graph kernels," *Applied Network Science*, vol. 5, no. 1, pp. 1–42, 2020.
- [39] L. E. Peterson, "K-nearest neighbor," *Scholarpedia*, vol. 4, no. 2, p. 1883, 2009.
- [40] W. S. Noble, "What is a support vector machine?" *Nature Biotechnology*, vol. 24, no. 12, pp. 1565–1567, 2006.
- [41] K. Riesen and H. Bunke, *Graph classification and clustering based on vector space embedding*. World Scientific, 2010, vol. 77.
- [42] P. Erdős and A. Rényi, "On the evolution of random graphs," *Publ. Math. Inst. Hung. Acad. Sci.*, vol. 5, no. 1, pp. 17–60, 1960.
- [43] R. Albert, H. Jeong, and A.-L. Barabási, "Diameter of the world-wide web," *Nature*, vol. 401, no. 6749, pp. 130–131, 1999.
- [44] M. Faloutsos, P. Faloutsos, and C. Faloutsos, "On power-law relationships of the internet topology," *ACM SIGCOMM Computer Communication Review*, vol. 29, no. 4, pp. 251–262, 1999.
- [45] C. Morris, N. M. Kriege, F. Bause, K. Kersting, P. Mutzel, and M. Neumann, "Tudataset: A collection of benchmark datasets for learning with graphs," in *ICML 2020 Workshop on Graph Representation Learning and Beyond (GRL+ 2020)*, 2020.
- [46] A. Di Martino, D. O'connor, B. Chen, K. Alaerts, J. S. Anderson, M. Assaf, J. H. Balsters, L. Baxter, A. Beggiato, and S. Bernaerts, "Enhancing studies of the connectome in autism using the autism brain imaging data exchange ii," *Scientific Data*, vol. 4, no. 1, pp. 1–15, 2017.
- [47] A. Schaefer, R. Kong, E. M. Gordon, T. O. Laumann, X. N. Zuo, A. J. Holmes, S. B. Eickhoff, and B. T. T. Yeo, "Local-global parcellation of the human cerebral cortex from intrinsic functional connectivity mri," *Cereb Cortex*, vol. 28, no. 9, pp. 3095–3114, 2018.
- [48] Y. Li, N. Wang, H. Wang, Y. Lv, Q. Zou, and J. Wang, "Surface-based single-subject morphological brain networks: Effects of morphological index, brain parcellation and similarity measure, sample size-varying stability and test-retest reliability," *NeuroImage*, vol. 235, p. 118018, 2021.
- [49] H. Wu, H. Wang, and L. Lü, "Individual t1-weighted/t2-weighted ratio brain networks: Small-worldness, hubs and modular organization," *International Journal of Modern Physics C*, vol. 29, no. 05, p. 1840007, 2018.
- [50] S. K. Panda and P. K. Jana, "Efficient task scheduling algorithms for heterogeneous multi-cloud environment," *The Journal of Supercomputing*, vol. 71, no. 4, pp. 1505–1533, 2015.